Electric-field-induced deformation dynamics of a single nematic disclination

Angela Vella,[1] Romuald Intartaglia,[1] Christophe Blanc,[1] Ivan I. Smalyukh,[2] Oleg D. Lavrentovich,[2] and Maurizio Nobili[1]
[1]*GDPC (UMR 5581) CNRS, Université de Montpellier-II, CC026, Place Eugéne Bataillon, F-34095 Montpellier Cedex 05, France*
[2]*Chemical Physics Interdisciplinary Program and Liquid Crystal Institute, Kent State University, Kent, Ohio 44242, USA*
Received 7 May 2004; revised manuscript received 11 November 2004; published 17 June 2005

Disclinations in nematic liquid crystals usually adopt a straight shape in order to minimize their elastic energy. Once created in the course of a nonequilibrium process such as a temperature quench from the isotropic to the nematic phase, the topologically stable disclinations of half-integer strength either annihilate each other in pairs of opposite strength or form topologically unstable disclinations of integer strength. In this article, we demonstrate that the annihilation process can be inhibited and the defects can be deformed by an applied electric field. We study the disclination lines in the deep uniaxial nematic phase, located at the boundary between two different types of walls, the so-called π wall a planar soliton stabilized by the surface anchoring

isotropy of the nematic elasticity. The increased total disclination length is over-compensated by the energy decrease due to the conversion of the high energy splay-bend deformation into the lower energy twist [13–15].

As far as we know, the deformation dynamics of an isolated disclination remains largely unexplored. The aim of this paper is to describe the deformation dynamics of a single disclination under an external electric field.

Straight disclinations orthogonal to the cell parallel plates are formed by a rapid quench from the isotropic phase. The nematic director in the cell is uniformly oriented along the parallel planar easy axes of the two substrates. The elastic energy excess, due to the presence of the disclinations, and the related excess of anchoring energy on the confinement substrates force the line defects to annihilate by pairs [7]. If a destabilizing electric field parallel to the disclinations is applied, the dynamics of annihilation is strongly modified. At electric fields E larger than the Frederiks threshold E_F, segments of BL walls appear and connect disclinations of opposite signs. The annihilation is more and more dampened for increasing fields and even stops at a critical field $E_C \approx 2E_F$ for which the two defects are immobilized. In the explored field range $E \approx E_C$, two different dynamical regimes are observed.

At temperatures T close to the isotropic-nematic transition temperature T_{NI} ($\Delta T = T_{NI} - T < 2\ ^\circ\mathrm{C}$), the line defect is only weakly deformed by the electric field. It moves as a whole by remaining almost straight and orthogonal to the substrates. In this regime, the line displacement is controlled by the surface energy change, and displays a complex dynamics. The study of such a regime will be published in a forthcoming paper.

In the second regime, at lower temperature, the line remains pinned with its two ends on each substrates. The dynamics does not imply surface changes but only bulk deformation. Under the re-

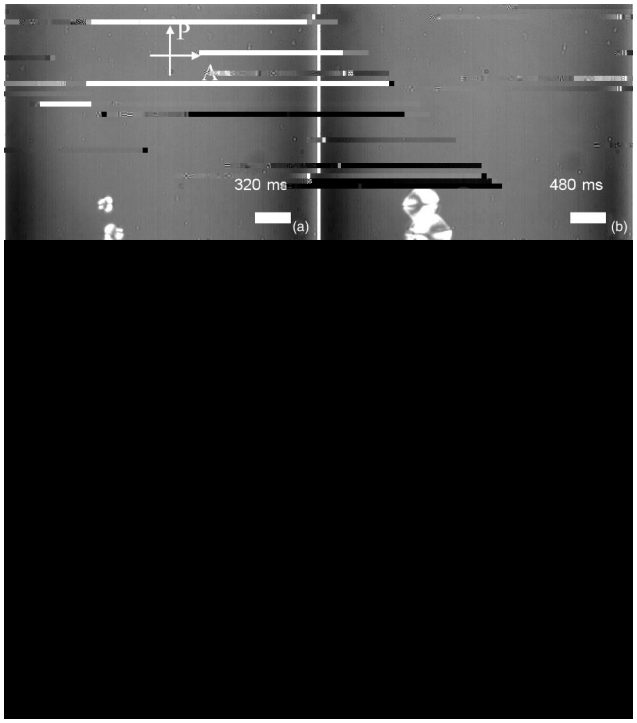

FIG. 1. Nucleation of the nematic phase of 5CB after a quench from the isotropic phase into a cell with planar anchoring and formation of disclinations connected by π walls see text . Thickness of the cell 11 μm. Bar 40 μm. T=33.5 °C.

B. General observations

The sample in the nematic phase is aligned along the two parallel easy axes at the chosen temperature $T=T_{NI}-\Delta T$. A short pulse of hot air is injected into the oven, which increases the sample temperature above T_{NI}. The sample becomes isotropic but after a few seconds the temperature decreases and droplets of nematic phase nucleate and grow Fig. 1 . Depending on the director orientation on the surface of neighboring droplets, disclinations may appear when droplets coalesce. Figure 2 shows a top view of a $-1/2$, $+1/2$ disclination pair. Two superposed surface walls are also created between them during this process. Note that these walls are not necessarily straight. The disclinations are situated at the ends of the surface walls and appear as points in a top view they are parallel to the light path and orthogonal to the two surfaces . This orientation is induced by the confinement and the strong planar anchoring conditions. Each surface wall corresponds to a continuous π-rotation of the director on the surface as proved by the presence of two bright fringes under crossed polarizers in Fig. 2. As the director turns by π, between two equivalent states, these walls are topologically stable, as long as the in-plane surface anchoring remains nonzero; they represent what are called the planar solitons 19 or the π walls. The annihilation dynamics of pair of opposite sign disclinations is driven by the elastic energy excess associated with these π walls 7 .

If an electric field parallel to the disclinations is applied before their annihilation, their dynamics is strongly affected. Above the Fréedericksz threshold E_F, a splay-bend director

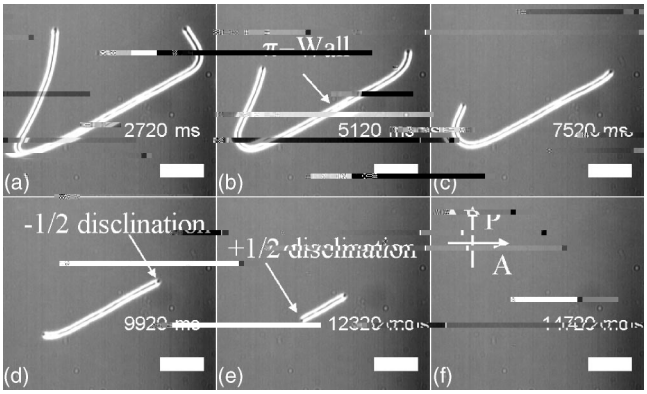

FIG. 2. Annihilation of a pair of $\pm 1/2$ disclinations under crossed polarizers electric field off . The disclinations are situated on the end tips of the topological wall the two bright fringes , whose formation is shown in Fig. 1. Each end tip represents the projection of a line defect orthogonal to the substrates. Cell thickness is 11 μm. Bar 40 μm. T=33.5 °C. Time between frames 2400 ms.

distortion develops in the cell. Due to the quadratic dielectric coupling $\mathbf{E}\cdot\hat{\mathbf{n}}^2$, the equilibrium distorted state is twofold degenerate. Domains characterized by one of the two equilibrium textures appear. Two adjacent domains are separated by a bulk distortion wall called a Brochard-Léger wall 8,9 . In the presence of disclination pairs, segments of BL wall connect defects of opposite charge see Fig. 3 b . In the case of an isolated pair, a mixed loop made by a BL wall and a π wall frequently forms Fig. 3 d .

The annihilation process is inhibited for a critical field E_C $E_C \approx 2E_F$. Figure 4 shows the defect behavior when $E < E_C$: the π wall retracts in favor of the BL wall 11,20 . During the relaxation, the defect lines remain almost straight and orthogonal to the substrates, which is similar to the relaxation without electric field 7 . After the defect annihilation, in the case of a single mixed loop, this latter is transformed into a regular BL wall 8,9 see Fig. 4 d , which finally relaxes.

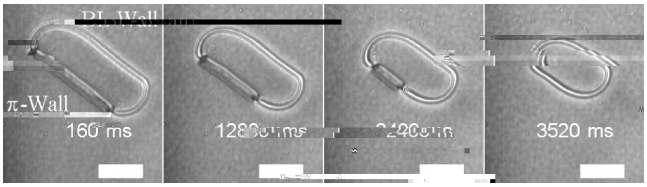

FIG. 4. Annihilation of a pair of $\pm 1/2$ disclinations in the presence of an electric field $E=0.2$ V μm^{-1}. Bar 40 μm. Thickness of sample 11 μm. $\Delta T \approx 3$ °C.

At high field $E > E_C$ and at high temperature $\Delta T < 2$ °C , the defect velocity is reversed with respect to the low field case: the BL wall is now converted to a π wall [10,11] as shown in Fig. 5. The final state after the defect annihilation consists in two surface π loops, one on each surface [Fig. 5 (d)]. Differently from a BL loop, these loops do not disappear after the electric field is switched off. In the two regimes presented so far [low field or high temperature], the two defect ends move with respect to the substrates and the elastic driving force depends on the anchoring energy.

At low temperature $\Delta T > 2$ °C a different type of dynamics is observed. A region β appears between the π and the BL walls as shown in Fig. 6. This β region corresponds to a strong deformation of the initially straight disclination [see Figs. 7 and 8]. The BL wall length decreases in favor of the β region, keeping unchanged the π wall length.

The rest of the paper is dedicated to the study of the single disclination deformation [region β] and its dynamical behavior. In particular, the line is first bent with an electric field larger than the critical one. Then, the bending [positive velocity] and the unbending [negative velocity] dynamic are measured as function of the field. Because segments of BL walls move very easily and BL loops shrink rapidly [they involve only bulk deformation], the quantitative study of the dynamics of a $\pm 1/2$ disclination along a BL wall is usually affected by the lateral motion of the wall. We therefore observe its motion along very large mixed loops [mean radius $R \gg 100$ μm]. The almost straight BL walls [see Fig. 6] are indeed motionless compared to the typical disclinations dynamics. The digitized images of the motion are then analyzed with a home-made program in order to obtain the position of the defect along the wall as a function of time.

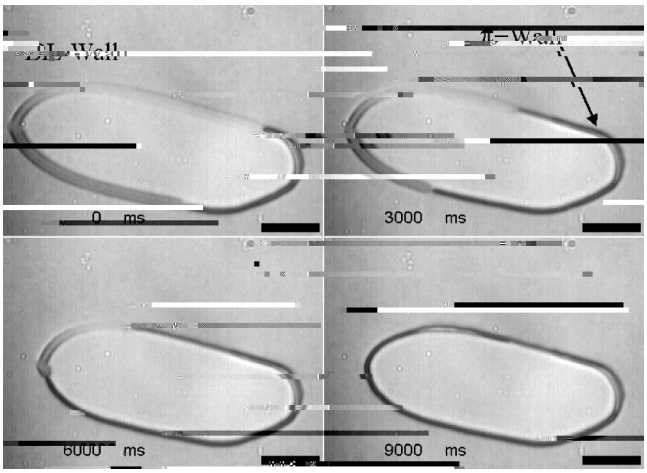

FIG. 5. Annihilation of a pair of $\pm 1/2$ disclinations in a mixed loop for large electric fields $E > E_C$ and high temperature $\Delta T < 2$ °C. The BL wall disappears and two stable π loops are formed at the end [one on each surface]. Bar 40 μm. Thickness of sample 11 μm. $\Delta T \approx 1$ °C.

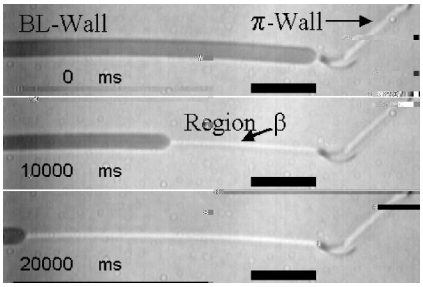

FIG. 6. Appearance of a region β between the π wall and the BL wall for electric fields larger than E_C. This region increases at the expense of the BL wall. Cell thickness is 11 μm. Bar 40 μm. $\Delta T = 3$ °C.

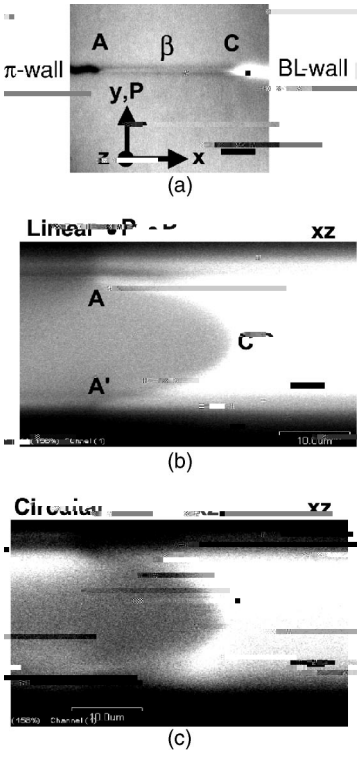

FIG. 7. Characterization of a $+1/2$ disclination bending behavior under electric field by FCPM. The surface easy axes are parallel to the y axis. [a] xy scan in the plane $z=d/2$ [middle of the cell]. We used linear polarization $\hat{\mathbf{P}}$ parallel to the $\hat{\mathbf{y}}$ axis. The region β between the π and BL walls is the disclination bending region. [b] xz scan in the plane containing the π and BL walls. The polarization is the same as in [a]. C is the inversion point of the bending deformation of the disclination. [c] xz scan in the same region as [b] with circular polarization. The bar in each picture is 5 μm. T=25 °C.

III. HALF-INTEGER DISCLINATION BENDING UNDER AN EXTERNAL ELECTRIC FIELD

Figure 7 shows a typical behavior of $+1/2$ disclination under an external electric field measured by FCPM. To characterize this region by the FCPM technique, we freeze this texture once obtained at $E > E_C$ by decreasing the field to $E = E_C$. Figure 7 a shows an *xy* scan. The polarization of the probing light has been chosen along the *y* axis easy axis in order to increase the contrast between the π and BL walls. The large fluorescent intensity from the BL wall proves that the director in this region is oriented in the *yz* plane with a

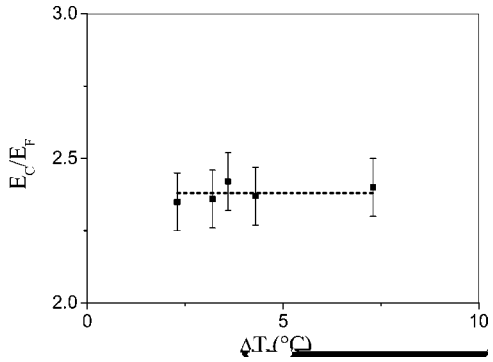

FIG. 11. $\tilde{E}=E_C/E_F$ as a function of $\Delta T=35.3\,°C-T$ for a cell thickness $d=11\ \mu$m. The points are the experimental data and the line is the average $\tilde{E}$ value.

the electric field amplitude around E_C. Each measurement begins 1 s after the electric field amplitude change. The motion is uniform. Figure 10 shows the dependence of the C velocity v on the effective applied field E for different sample temperatures. Note that v depends linearly on the field in the studied range of values. The threshold field E_C decreases with increasing temperature whereas the velocity susceptibility to the electric field $\alpha=dv/dE$ is almost temperature independent.

In Fig. 11 the critical field $\tilde{E}_C=E_C/E_F$ normalized to the Fréedericksz field E_F is plotted versus ΔT. E_C has been obtained from the best fit of the data points in Fig. 10 whereas E_F has been directly measured on the same cell region in order to minimize the errors due to the cell thickness inhomogeneities.

The ratio $\tilde{E}_C$ is found independent of the sample temperature, which shows that the stabilization field scales as the Fréedericksz field when the temperature changes. Concerning the dependence on the cell thickness, Fig. 12 shows that $\tilde{E}_C$ increases with increasing thickness in the 10–50 μm range.

The velocity susceptibility to the electric field α is however almost independent of the thickness d and the sample temperature, as shown in Figs. 13 and 14, respectively.

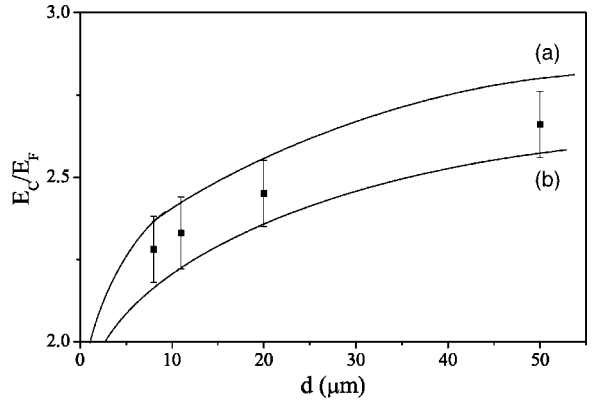

FIG. 12.9 ΔTT

IV. MODEL

In the regime of large disclination deformations presented in Sec. III, the experimental line profile is similar to the one shown in Fig. 9. The line is therefore composed of three main parts: the first one AB is parallel and very close to the upper substrate, the second one BB' is almost perpendicular to the surfaces and is weakly bent, and, finally, the third one $B'A'$ barely visible in Fig. 9 is close and parallel to the lower surface. Experimentally we observe the part BB' remains weakly bent during the stretching and unstretching of the line. To model our system, we assume the part BB' changes only its location but not its shape and the segments AB and $A'B'$ change their length. In this approximation, the disclination deformation is driven by a conversion of the BL wall elastic energy into the energy of two parallel disclinations. Applying the virtual work principle, the driving elastic force on the disclination F_{el} is given by

$$F_v = 2bv\, d\eta_\beta \qquad 15$$

where $\eta_\beta = \gamma_1 - \alpha_2^2 / 2\ \eta_\beta - \gamma_2$ 6 is an effective viscosity which takes into account in an empiric way the backflow effects. The parameters γ_1, α_2, η_β, and

Phys. Rev. Lett. **58**, 222 1987 .
7 A. Bogi, P. Martinot-Lagarde, I. Dozov, and M. Nobili, Phys. Rev. Lett. **89**, 225501 2002 .
8 F. Brochard, J. Phys. Paris **33**, 607 1972 .
9 L. Leger, Mol. Cryst. Liq. Cryst. **24**, 33 1973 .
10 A. Stieb, G. Baur, and M. Meier, J. Phys. Paris **36**, C1 1975 .
11 K. S. Krishnamurthy and R. Balakrishnan, Liq. Cryst. **29**, 383 2002 .
12 J. Ignès-Mullol, J. Baudry, L. Lejcek, and P. Oswald, Phys. Rev. E **59**, 568 1999 .
13 M. Mihailovic and P. Oswald, J. Phys. Paris **49**, 1467 1988 .
14 Y. Galerne, J. Itoua, and L. Liebert, J. Phys. Paris **49**, 681 1988 .
15 C. Chevallard, M. Clerc, P. Coullet, and J. Gilli, Europhys. Lett. **58**, 686 2002 .
16 B. A. Belyaev, N. A. Drokin, V. F. Shabanov, and V. N. Shepov, Mol. Cryst. Liq. Cryst. Sci. Technol., Sect. A **366**, 2157 2001 .
17 I. I. Smalyukh, S. V. Shiyanovskii, and O. D. Lavrentovich, Chem. Phys. Lett. **336**, 88 2001 .
18 S. V. Shiyanovskii, I. I. Smalyukh, and O. D. Lavrentovich, in *Defects in Liquid Crystals: Computer Simulations, Theory and Experiments*, edited by O. D. Lavrentovich, P. Pasini, C. Zannoni, and S. Zumer, NATO Science Series Kluwer Academic Publishers, Dordrecht, 2001 , pp. 229–270.
19 M. Kleman and O. Lavrentovich, *Soft Matter Physics: An Introduction* Springer, New York, 2003 , Chap. 12.4.1.
20 C. Chevallard, Ph.D. thesis, Université de Nice, 1985 unpublished .
21 At large fields $E \approx E_C = 2E_F$ this approximation is still relevant. If we compare the exact free energy and the one obtained by taking into account only the first mode of the expansion, the relative error remains quite small $\sim 16\%$.
22 S. Chandrasekhar and G. S. Ranganath, Adv. Phys. **35**, 507 1986 .
23 E. B. Priestley, P. J. Wojtowicz, and P. Sheng, *Introduction to Liquid Crystals* Plenum, New York, 1974 , Chap. 10, pp. 151-161.
24 For a surface-disclination distance of a few micrometers as measured in Fig. 9 parts AB and AB′ , the disclination elastic energy change due to the anchoring remains relatively small $\sim 10\%$ compared to the one in Eq. 9 .
25 R. B. Meyer, Solid State Commun. **12**, 585 1973 .
26 J. D. Bunning, T. E. Faber, and P. L. Sherrel, J. Phys. I **42**, 1175 1991 .
27 B. R. Ratna and P. Shashidhar, Mol. Cryst. Liq. Cryst. **42**, 113 1977 .
28 K. Skarp, S. Lagerwall, and B. Stebler, Mol. Cryst. Liq. Cryst. **60**, 215 1980 .